DESY 01-225 ISSN 0418-9833
December 2001

Measurement of Dijet Cross Sections in Photoproduction at HERA

H1 Collaboration

Abstract

Dijet cross sections as functions of several jet observables are measured in photoproduction using the H1 detector at HERA. The data sample comprises e^+p data with an integrated luminosity of 34.9 pb^{-1}. Jets are selected using the inclusive $k_\perp$ algorithm with a minimum transverse energy of 25 GeV for the leading jet. The phase space covers longitudinal proton momentum fraction x_p and photon longitudinal momentum fraction x_γ in the ranges $0.05 < x_p < 0.6$ and $0.1 < x_\gamma < 1$. The predictions of next-to-leading order perturbative QCD, including recent photon and proton parton densities, are found to be compatible with the data in a wide kinematical range.

To be submitted to Eur. Phys. J. C

C. Adloff[33], V. Andreev[24], B. Andrieu[27], T. Anthonis[4], V. Arkadov[35], A. Astvatsatourov[35], A. Babaev[23], J. Bähr[35], P. Baranov[24], E. Barrelet[28], W. Bartel[10], J. Becker[37], A. Beglarian[34], O. Behnke[13], C. Beier[14], A. Belousov[24], Ch. Berger[1], T. Berndt[14], J.C. Bizot[26], J. Böhme[10], V. Boudry[27], W. Braunschweig[1], V. Brisson[26], H.-B. Bröker[2], D.P. Brown[10], W. Brückner[12], D. Bruncko[16], J. Bürger[10], F.W. Büsser[11], A. Bunyatyan[12,34], A. Burrage[18], G. Buschhorn[25], L. Bystritskaya[23], A.J. Campbell[10], S. Caron[1], F. Cassol-Brunner[22], D. Clarke[5], C. Collard[4], J.G. Contreras[7,41], Y.R. Coppens[3], J.A. Coughlan[5], M.-C. Cousinou[22], B.E. Cox[21], G. Cozzika[9], J. Cvach[29], J.B. Dainton[18], W.D. Dau[15], K. Daum[33,39], M. Davidsson[20], B. Delcourt[26], N. Delerue[22], R. Demirchyan[34], A. De Roeck[10,43], E.A. De Wolf[4], C. Diaconu[22], J. Dingfelder[13], P. Dixon[19], V. Dodonov[12], J.D. Dowell[3], A. Droutskoi[23], A. Dubak[25], C. Duprel[2], G. Eckerlin[10], D. Eckstein[35], V. Efremenko[23], S. Egli[32], R. Eichler[36], F. Eisele[13], E. Eisenhandler[19], M. Ellerbrock[13], E. Elsen[10], M. Erdmann[10,40,e], W. Erdmann[36], P.J.W. Faulkner[3], L. Favart[4], A. Fedotov[23], R. Felst[10], J. Ferencei[10], S. Ferron[27], M. Fleischer[10], P. Fleischmann[10], Y.H. Fleming[3], G. Flügge[2], A. Fomenko[24], I. Foresti[37], J. Formánek[30], G. Franke[10], G. Frising[1], E. Gabathuler[18], K. Gabathuler[32], J. Garvey[3], J. Gassner[32], J. Gayler[10], R. Gerhards[10], C. Gerlich[13], S. Ghazaryan[4,34], L. Goerlich[6], N. Gogitidze[24], C. Grab[36], V. Grabski[34], H. Grässler[2], T. Greenshaw[18], G. Grindhammer[25], T. Hadig[13], D. Haidt[10], L. Hajduk[6], J. Haller[13], W.J. Haynes[5], B. Heinemann[18], G. Heinzelmann[11], R.C.W. Henderson[17], S. Hengstmann[37], H. Henschel[35], R. Heremans[4], G. Herrera[7,44], I. Herynek[29], M. Hildebrandt[37], M. Hilgers[36], K.H. Hiller[35], J. Hladký[29], P. Höting[2], D. Hoffmann[22], R. Horisberger[32], A. Hovhannisyan[34], S. Hurling[10], M. Ibbotson[21], Ç. İşsever[7], M. Jacquet[26], M. Jaffre[26], L. Janauschek[25], X. Janssen[4], V. Jemanov[11], L. Jönsson[20], C. Johnson[3], D.P. Johnson[4], M.A.S. Jones[18], H. Jung[20,10], D. Kant[19], M. Kapichine[8], M. Karlsson[20], O. Karschnick[11], F. Keil[14], N. Keller[37], J. Kennedy[18], I.R. Kenyon[3], S. Kermiche[22], C. Kiesling[25], P. Kjellberg[20], M. Klein[35], C. Kleinwort[10], T. Kluge[1], G. Knies[10], B. Koblitz[25], S.D. Kolya[21], V. Korbel[10], P. Kostka[35], S.K. Kotelnikov[24], R. Koutouev[12], A. Koutov[8], H. Krehbiel[10], J. Kroseberg[37], K. Krüger[10], T. Kuhr[11], T. Kurča[16], D. Lamb[3], M.P.J. Landon[19], W. Lange[35], T. Laštovička[35,30], P. Laycock[18], E. Lebailly[26], A. Lebedev[24], B. Leißner[1], R. Lemrani[10], V. Lendermann[7], S. Levonian[10], M. Lindstroem[20], B. List[36], E. Lobodzinska[10,6], B. Lobodzinski[6,10], A. Loginov[23], N. Loktionova[24], V. Lubimov[23], S. Lüders[36], D. Lüke[7,10], L. Lytkin[12], H. Mahlke-Krüger[10], N. Malden[21], E. Malinovski[24], I. Malinovski[24], S. Mangano[36], R. Maraček[25], P. Marage[4], J. Marks[13], R. Marshall[21], H.-U. Martyn[1], J. Martyniak[6], S.J. Maxfield[18], D. Meer[36], A. Mehta[18], K. Meier[14], A.B. Meyer[11], H. Meyer[33], J. Meyer[10], P.-O. Meyer[2], S. Mikocki[6], D. Milstead[18], T. Mkrtchyan[34], S. Mohrdieck[11], M.N. Mondragon[7], F. Moreau[27], A. Morozov[8], J.V. Morris[5], K. Müller[37], P. Murín[16,42], V. Nagovizin[23], B. Naroska[11], J. Naumann[7], Th. Naumann[35], G. Nellen[25], P.R. Newman[3], F. Niebergall[11], C. Niebuhr[10], O. Nix[14], G. Nowak[6], J.E. Olsson[10], D. Ozerov[23], V. Panassik[8], C. Pascaud[26], G.D. Patel[18], M. Peez[22], E. Perez[9], A. Petrukhin[35], J.P. Phillips[18], D. Pitzl[10], R. Pöschl[26], I. Potachnikova[12], B. Povh[12], G. Rädel[1], J. Rauschenberger[11], P. Reimer[29], B. Reisert[25], D. Reyna[10], C. Risler[25], E. Rizvi[3], P. Robmann[37], R. Roosen[4], A. Rostovtsev[23], S. Rusakov[24], K. Rybicki[6], D.P.C. Sankey[5], S. Schätzel[13], J. Scheins[1], F.-P. Schilling[10], P. Schleper[10], D. Schmidt[33], D. Schmidt[10], S. Schmidt[25], S. Schmitt[10], M. Schneider[22], L. Schoeffel[9], A. Schöning[36], T. Schörner[25], V. Schröder[10], H.-C. Schultz-Coulon[7], C. Schwanenberger[10], K. Sedlák[29], F. Sefkow[37], V. Shekelyan[25], I. Sheviakov[24], L.N. Shtarkov[24], Y. Sirois[27], T. Sloan[17], P. Smirnov[24], Y. Soloviev[24], D. South[21], V. Spaskov[8], A. Specka[27], H. Spitzer[11], R. Stamen[7], B. Stella[31],

J. Stiewe[14], U. Straumann[37], M. Swart[14], S. Tchetchelnitski[23], G. Thompson[19], P.D. Thompson[3], N. Tobien[10], F. Tomasz[14], D. Traynor[19], P. Truöl[37], G. Tsipolitis[10,38], I. Tsurin[35], J. Turnau[6], J.E. Turney[19], E. Tzamariudaki[25], S. Udluft[25], M. Urban[37], A. Usik[24], S. Valkár[30], A. Valkárová[30], C. Vallée[22], P. Van Mechelen[4], S. Vassiliev[8], Y. Vazdik[24], A. Vichnevski[8], K. Wacker[7], J. Wagner[10], R. Wallny[37], B. Waugh[21], G. Weber[11], M. Weber[14], D. Wegener[7], C. Werner[13], N. Werner[37], M. Wessels[1], G. White[17], S. Wiesand[33], T. Wilksen[10], M. Winde[35], G.-G. Winter[10], Ch. Wissing[7], M. Wobisch[10], E.-E. Woehrling[3], E. Wünsch[10], A.C. Wyatt[21], J. Žáček[30], J. Zálešák[30], Z. Zhang[26], A. Zhokin[23], F. Zomer[26], and M. zur Nedden[10]

[1] *I. Physikalisches Institut der RWTH, Aachen, Germany*[a]
[2] *III. Physikalisches Institut der RWTH, Aachen, Germany*[a]
[3] *School of Physics and Space Research, University of Birmingham, Birmingham, UK*[b]
[4] *Inter-University Institute for High Energies ULB-VUB, Brussels; Universiteit Antwerpen (UIA), Antwerpen; Belgium*[c]
[5] *Rutherford Appleton Laboratory, Chilton, Didcot, UK*[b]
[6] *Institute for Nuclear Physics, Cracow, Poland*[d]
[7] *Institut für Physik, Universität Dortmund, Dortmund, Germany*[a]
[8] *Joint Institute for Nuclear Research, Dubna, Russia*
[9] *CEA, DSM/DAPNIA, CE-Saclay, Gif-sur-Yvette, France*
[10] *DESY, Hamburg, Germany*
[11] *Institut für Experimentalphysik, Universität Hamburg, Hamburg, Germany*[a]
[12] *Max-Planck-Institut für Kernphysik, Heidelberg, Germany*
[13] *Physikalisches Institut, Universität Heidelberg, Heidelberg, Germany*[a]
[14] *Kirchhoff-Institut für Physik, Universität Heidelberg, Heidelberg, Germany*[a]
[15] *Institut für experimentelle und Angewandte Physik, Universität Kiel, Kiel, Germany*
[16] *Institute of Experimental Physics, Slovak Academy of Sciences, Košice, Slovak Republic*[e,f]
[17] *School of Physics and Chemistry, University of Lancaster, Lancaster, UK*[b]
[18] *Department of Physics, University of Liverpool, Liverpool, UK*[b]
[19] *Queen Mary and Westfield College, London, UK*[b]
[20] *Physics Department, University of Lund, Lund, Sweden*[g]
[21] *Physics Department, University of Manchester, Manchester, UK*[b]
[22] *CPPM, CNRS/IN2P3 - Univ Mediterranee, Marseille - France*
[23] *Institute for Theoretical and Experimental Physics, Moscow, Russia*[l]
[24] *Lebedev Physical Institute, Moscow, Russia*[e]
[25] *Max-Planck-Institut für Physik, München, Germany*
[26] *LAL, Université de Paris-Sud, IN2P3-CNRS, Orsay, France*
[27] *LPNHE, Ecole Polytechnique, IN2P3-CNRS, Palaiseau, France*
[28] *LPNHE, Universités Paris VI and VII, IN2P3-CNRS, Paris, France*
[29] *Institute of Physics, Academy of Sciences of the Czech Republic, Praha, Czech Republic*[e,i]
[30] *Faculty of Mathematics and Physics, Charles University, Praha, Czech Republic*[e,i]
[31] *Dipartimento di Fisica Università di Roma Tre and INFN Roma 3, Roma, Italy*
[32] *Paul Scherrer Institut, Villigen, Switzerland*
[33] *Fachbereich Physik, Bergische Universität Gesamthochschule Wuppertal, Wuppertal, Germany*
[34] *Yerevan Physics Institute, Yerevan, Armenia*

[35] *DESY, Zeuthen, Germany*
[36] *Institut für Teilchenphysik, ETH, Zürich, Switzerland*[j]
[37] *Physik-Institut der Universität Zürich, Zürich, Switzerland*[j]

[38] *Also at Physics Department, National Technical University, Zografou Campus, GR-15773 Athens, Greece*
[39] *Also at Rechenzentrum, Bergische Universität Gesamthochschule Wuppertal, Germany*
[40] *Also at Institut für Experimentelle Kernphysik, Universität Karlsruhe, Karlsruhe, Germany*
[41] *Also at Dept. Fis. Ap. CINVESTAV, Mérida, Yucatán, México*[k]
[42] *Also at University of P.J. Šafárik, Košice, Slovak Republic*
[43] *Also at CERN, Geneva, Switzerland*
[44] *Also at Dept. Fis. CINVESTAV, México City, México*[k]

[a] *Supported by the Bundesministerium für Bildung und Forschung, FRG, under contract numbers 05 H1 1GUA /1, 05 H1 1PAA /1, 05 H1 1PAB /9, 05 H1 1PEA /6, 05 H1 1VHA /7 and 05 H1 1VHB /5*
[b] *Supported by the UK Particle Physics and Astronomy Research Council, and formerly by the UK Science and Engineering Research Council*
[c] *Supported by FNRS-FWO-Vlaanderen, IISN-IIKW and IWT*
[d] *Partially Supported by the Polish State Committee for Scientific Research, grant no. 2P0310318 and SPUB/DESY/P03/DZ-1/99 and by the German Bundesministerium für Bildung und Forschung*
[e] *Supported by the Deutsche Forschungsgemeinschaft*
[f] *Supported by VEGA SR grant no. 2/1169/2001*
[g] *Supported by the Swedish Natural Science Research Council*
[i] *Supported by the Ministry of Education of the Czech Republic under the projects INGO-LA116/2000 and LN00A006, by GA AVČR grant no B1010005 and by GAUK grant no 173/2000*
[j] *Supported by the Swiss National Science Foundation*
[k] *Supported by CONACyT*
[l] *Partially Supported by Russian Foundation for Basic Research, grant no. 00-15-96584*

1 Introduction

In QCD (Quantum Chromo Dynamics) the photoproduction of jets with high transverse energy is described by the hard interaction of real photons with quarks and gluons inside the proton. Interactions with two outgoing partons of large transverse momentum are due to direct processes, such as $\gamma q \rightarrow gq$ (QCD-Compton effect) and $\gamma g \rightarrow q\overline{q}$ (photon-gluon fusion) and resolved processes where the photon first splits into a quark pair (or higher multiplicity fluctuation) and one of the resulting partons subsequently scatters off a parton in the proton. The calculation of the latter processes can be approximated by ascribing parton densities to the photon, which also include the inherently non-perturbative aspects of the photon structure.

In analogy to the proton case parton densities of the photon depend on a factorization scale μ_γ and on x_γ, the longitudinal momentum fraction of the photon taken by the interacting parton. The limiting case of direct interactions is given by $x_\gamma = 1$. At HERA these photoproduction reactions can be investigated in inelastic electron (positron) proton reactions at very small squared four-momentum transfers Q^2. Starting from the first investigation of this kind at HERA [1] the comparison of the predictions of QCD with the results has been a central topic of interest [2–4]. These investigations are particularly interesting, because previous measurements of high transverse energy jet production in ep and $p\bar{p}$ scattering were not fully described by QCD calculations [5–7].

High transverse energy jets provide a natural hard scale for perturbative QCD calculations. Such calculations have been performed for direct and resolved processes in leading (LO) and next-to-leading (NLO) order. The measurement of jet cross sections at high transverse energy presented in this paper can therefore be used to test the current predictions of NLO perturbative QCD and the parameterizations of photon and proton parton densities at large scales with a precision of typically 10%. Photon quark densities have been determined in experiments at e^+e^--colliders [8] which investigate the photon structure function F_2^γ, where x_γ values up to 0.8 and scales up to $500\,\mathrm{GeV}^2$ have been reached. In comparison the analysis presented here extends the x_γ range up to 1 at scales between 600 and $6000\,\mathrm{GeV}^2$, where the quark density parameterizations of the photon are presently not well constrained by measurements. In contrast to the F_2^γ measurements, the photoproduction of jets is directly sensitive to the gluon density of the photon, which is poorly known to date. Furthermore our data are sensitive to the parton densities of the proton at fractional momentum values x_p up to 0.6. In this kinematical regime, the quark densities are well known from deeply inelastic scattering data, while the gluon density has uncertainties of the order 10 to 50% [9]. Photoproduction data can thus be used to constrain the parton density functions in regions where only few measurements are presently available. However, detailed parton densities can not be extracted from these data alone.

This paper is based on an e^+p data sample collected with the H1 detector in the years 1995-1997 and corresponds to an integrated luminosity of 34.9 pb^{-1}. It presents dijet cross sections as a function of jet observables with mean jet transverse energies $20 < E_T < 80\,\mathrm{GeV}$, observed x_γ values $0.1 < x_\gamma < 1$ and values of x_p ranging from 0.05 to 0.6. The two jets considered in the investigated process $ep \rightarrow e\,\mathrm{jet}\,\mathrm{jet}\,X$ are defined as the two jets with the highest transverse energy[1].

[1] A similar analysis has recently been made available [10].

2 Jets in Photoproduction

2.1 Cross sections and observables

The cross section for the photoproduction of hard jets in electron-proton collisions, σ_{ep}, can be calculated from the photon-proton scattering result, $\sigma_{\gamma p}$, using the factorization ansatz

$$\sigma_{ep\to eX} = \int \mathrm{d}y f_{\gamma,e}(y)\sigma_{\gamma p}(y) \ . \tag{1}$$

Here the usual variable y of deeply inelastic scattering is interpreted as the longitudinal momentum fraction of the incoming electron taken by the photon and $f_{\gamma,e}$ is the photon flux calculated in the Weizsäcker-Williams approximation [11–13]. The hadronic photon-proton jet cross section is obtained as the convolution of the partonic cross sections with the parton momentum distributions of the proton $f_{i/p}$ and the photon $f_{j/\gamma}$. As outlined in the introduction it is divided into a sum of two components, the direct part $\sigma_{\gamma p}^{\text{direct}}$, where the photon directly interacts with a parton of the proton and the resolved part $\sigma_{\gamma p}^{\text{resolved}}$, where one of the partons inside the photon interact with a parton of the proton. This distinction is unambiguously defined in leading order only and depends on the photon factorization scale μ_γ. The two components can be expressed as:

$$\sigma_{\gamma p}^{direct} = \sum_i \int \mathrm{d}x_p f_{i/p}(x_p,\mu_p)\hat{\sigma}_{i\gamma}(\hat{s},\mu_\gamma,\mu_p,\alpha_s(\mu_r),\mu_r) \tag{2}$$

$$\sigma_{\gamma p}^{resolved} = \sum_{j,i} \int \mathrm{d}x_\gamma f_{j/\gamma}(x_\gamma,\mu_\gamma)\mathrm{d}x_p f_{i/p}(x_p,\mu_p)\hat{\sigma}_{ij}(\hat{s},\mu_\gamma,\mu_p,\alpha_s(\mu_r),\mu_r) \ . \tag{3}$$

The squared centre-of-mass energy of the hard subprocess is $\hat{s} = x_p x_\gamma y s$, where $\sqrt{s}$ is the total centre-of-mass energy in the ep-system, i.e. 300 GeV for this analysis. The proton factorization scale is μ_p and the renormalization scale is μ_r. The partonic cross sections $\hat{\sigma}$ can be expanded as a perturbative series in powers of α_s and have been calculated up to the next-to-leading order in QCD [14–17].

The total cross sections on the left hand side of equation 1 are obtained by integrating over y, x_p and x_γ. The partonic cross sections $\hat{\sigma}_{i\gamma}$ and $\hat{\sigma}_{ij}$ contain a further integration over an internal degree of freedom, e.g. $\cos\theta^*$, the scattering angle in the centre-of-mass system of the partonic two body reaction, or the transverse energy. More detailed information on the reaction dynamics is obtained by measuring differential cross sections in these kinematical observables. In order to avoid singularities in the partonic cross sections a minimum cut in θ^* or in the transverse energy of the outgoing partons has to be applied.

The two scaled longitudinal parton momenta x_γ and x_p are calculated from the jets produced in the hard subprocess, using the definition

$$x_\gamma = \frac{1}{2E_e y}(E_{T,1}e^{-\eta_1} + E_{T,2}e^{-\eta_2}) \tag{4}$$

$$x_p = \frac{1}{2E_p}(E_{T,1}e^{\eta_1} + E_{T,2}e^{\eta_2}) \tag{5}$$

Here $E_{T,1}$ and $E_{T,2}$ are the transverse energies of the two jets of the hard subprocess, η_1 and η_2 are their pseudorapidities in the laboratory frame ($\eta = -\ln(\tan\theta/2)$) and E_e and E_p are the energies of the electron and proton beams[2]. These relations are used as definitions of observables in all orders and are easily derived for $2 \to 2$ processes, where the transverse energies of the jets are equal. The pseudorapidities of the jets are related to θ^* via

$$\cos\theta^* = |\tanh((\eta_1 - \eta_2)/2)| \ . \tag{6}$$

In principle one could measure the dependence of the fourfold differential cross section $d\sigma_{\gamma p}/dydx_\gamma dx_p d\cos\theta^*$ on all four variables. This, however, would require a much larger data set than presently available. Therefore in this paper more inclusive quantities are presented. The distribution of the invariant mass of the two jets with the highest transverse energies, M_{JJ}, the mean transverse energy of the two leading jets $E_{T,mean}$ and the transverse energy distribution of the highest transverse energy jet, $E_{T,max}$, are studied. The cross section differential in the average value of the pseudorapidities $\overline{\eta} = (\eta_1 + \eta_2)/2$ is particularly sensitive to parton density functions. It is thus presented for different photon-proton centre-of-mass energies (y regions) and different scales ($E_{T,max}$ regions), cf. equations 4 and 5.

Differential cross sections in x_γ and x_p are measured in different scale regions ($E_{T,max}$ regions) and for different x_γ or x_p cut-off values. The angle θ^* is sensitive to the dynamics of jet production and the corresponding differential cross section is therefore evaluated for different x_γ regions for all M_{JJ} and in addition with a cut in M_{JJ}. The $\cos\theta^*$ distribution could be influenced by the production of W or Z^0 bosons, whose hadronic decays have a different angular distribution from that expected for QCD dijet production. Using the EPVEC Monte Carlo generator [18], the contribution of W bosons is estimated to be 5-6 events. The Z^0 contribution is expected to be negligible. The background from these processes is therefore not considered in the following.

In the present analysis jets are defined using the inclusive $k_\perp$ algorithm as proposed in [19, 20]. The application of this algorithm has become standard in jet analyses at HERA [21]. It utilizes a definition of jets in which not all particles are assigned to hard jets. Here it is applied in the laboratory frame with the separation parameter set to 1 and using an E_T weighted recombination scheme in which the jets are considered massless.

2.2 QCD Predictions and Models

To simulate the direct and resolved photoproduction of jets, the PYTHIA 5.7 [22] and HERWIG 5.9 [23] event generators were used followed by a full detector simulation [24] of all Monte Carlo events. Both programs contain the Born level QCD hard scattering matrix elements, regulated by a minimum cut-off in transverse momentum. Leading logarithmic parton showers are used to represent higher order QCD radiation. GRV-LO [25, 26] parton density functions (pdfs) for the proton and photon were chosen. The Lund String model is applied in PYTHIA to hadronize the outgoing partons, while in HERWIG the cluster hadronization approach is used.

[2]The coordinate system is centered at the nominal interaction point with the positive z direction along the incident proton beam. The polar angle θ is defined with respect to the positive z axis.

Multiple interactions between the proton and the resolved photon are dealt with in PYTHIA by adding additional interactions between spectator partons within the same event. These processes are calculated by extending the perturbative parton-parton scattering to a low E_T cut-off.

In HERWIG multiple interactions are included by producing in a fraction P' of the resolved events so called *soft underlying events*. These interactions are parameterized using experimental results of soft hadron-hadron scattering. The effect of multiple interactions is tested by comparing, in the data and in the HERWIG calculations, the energy flow distributions around the jet axis with and without a fraction P' of events containing the soft underlying event. For P' $\sim$30-35% these distributions are found to be well described for all regions of x_γ. The difference of the calculated HERWIG cross sections with and without 35% of soft underlying events is below 10% for x_γ between 0.3-0.8 and 10-20% for $x_\gamma < 0.3$. For $x_\gamma > 0.8$ the difference is negligible. PYTHIA is also able to describe these distributions.

The goal of this analysis is the comparison of the measured cross sections to perturbative QCD calculations at the parton level. The LO and NLO dijet cross sections were computed using a program based on the subtraction method [14,27] for the analytic cancellation of infrared singularities. In calculating LO and NLO cross sections a 2-loop α_s was taken with 5 active flavours. Λ_{QCD} was set to 0.226 GeV ($\alpha_s(M_Z) = 0.118$), which is the value used in the proton parton density functions. CTEQ5M [28] parton density functions were chosen for the proton whereas MRST99 [29] parton density functions were selected to test the dependence of the NLO cross sections on the proton pdfs. For the photon we choose GRV-HO [30] as a main setting and the parameterization of AFG-HO [31] to study the dependence of the results on the choice of the photon pdfs. The renormalization scale μ_r and the factorization scales μ_p and μ_γ were, event by event, set to the sum of the transverse energies of the outgoing partons divided by two. The QCD program allows the variation of this common scale. It was varied from 0.5 to 2 times the default scale to estimate the scale uncertainty in the NLO calculation. This uncertainty turned out to vary between ± 10 and $\pm 20\%$ in the measured kinematic range.

In addition the data are compared to the predictions of NLO QCD corrected for hadronization effects, which are defined as the ratio of the cross sections with jets reconstructed from hadrons and from partons before hadronization. The hadronization effects are calculated with PYTHIA and HERWIG and the mean value of the two predictions is used for corrections. Here the difference between the two Monte Carlo models is in general very small and at maximum 10%. The jets built out of partons are found to be very well correlated with the jets built out of hadrons.

3 Experimental Technique

3.1 H1 Detector

The H1 detector is described in detail in [32,33]. Only those components relevant to the present analysis are briefly described here. The Liquid Argon (LAr) [34] and SpaCal [35] calorimeters were used to trigger events, to reconstruct the hadronic energy of the final state and to select photoproduction events by eliminating events with an identified scattered positron. The LAr

calorimeter covers the polar angle range $4^\circ < \theta < 154^\circ$ with full azimuthal acceptance. The jet energy calibration agrees at the 2% level with the Monte Carlo simulation as determined by the transverse energy balance between jet and electron for deeply inelastic scattering events and by the transverse energy balance between the two jets for the photoproduction sample in different kinematic regions. The angular region $153^\circ < \theta < 177.8^\circ$ is covered by the SpaCal, a lead/scintillating-fibre calorimeter. It has a hadronic energy scale uncertainty of 8%. The central tracking detector (CJC) was used to reconstruct the interaction vertex and to supplement the measurement of hadronic energy flow. The CJC consists of two concentric cylindrical drift chambers, coaxial with the beam-line, with a polar angle coverage of $15^\circ < \theta < 165^\circ$. The entire CJC is immersed in a 1.15 T magnetic field. The luminosity determination is based on the measurement of the $ep \to ep\gamma$ Bethe-Heitler process, where the positron and photon are detected in calorimeters located downstream of the interaction point in e-beam direction.

3.2 Event Selection

The data sample was collected at HERA with the H1 detector in the years 1995-97, when protons of 820 GeV energy collided with positrons of 27.6 GeV energy resulting in a centre-of-mass energy of 300 GeV. The events were triggered on the basis of high transverse energy deposits in the LAr calorimeter. The trigger efficiencies were above 94% for the event sample described in this analysis. Energy deposits in the calorimeters and tracks in the CJC were combined in a manner that avoids double counting to reconstruct the hadronic energy of events [36].

It was required that an event vertex was reconstructed within 35 cm of the nominal z position of the vertex. The most significant background in the data sample arises from neutral current deeply inelastic scattering events, and was suppressed by removing events with an electron identified in the LAr calorimeter or SpaCal and by requiring $y < 0.9$, with y reconstructed using hadronic variables [37]. This reduces the background to less than 1% for the total sample. In the region with the highest y at low $\overline{\eta}$ the remaining background was calculated to be about 5% based on deeply inelastic scattering dijet data and the ARIADNE [38] Monte Carlo interfaced with DJANGO [39]. It was subtracted statistically. After applying a cut on the missing transverse energy $E_{T,miss} < 20$ GeV the remaining charged current ($ep \to \nu X$) and non-ep scattering background was found to be negligible. Events induced by cosmic rays were removed.

Asymmetric cuts on the E_T of the two jets with the highest transverse energies are applied to avoid regions of phase space affected by uncertainties in the NLO calculation [14]. On the other hand a highly asymmetric cut causes large NLO corrections and a pronounced dependence on the choice of scale. The jet selection criteria therefore required an E_T of the highest transverse energy jet $E_{T,max} > 25$ GeV, and the transverse energy of the second highest transverse energy jet $E_{T,second} > 15$ GeV. When the cut on $E_{T,second}$ is varied between ± 5 GeV, the ratio of the measured cross sections to the theoretical prediction varies by up to 10% for $x_\gamma < 0.8$ and by up to 3% for $x_\gamma > 0.8$.

The pseudorapidity of each jet η_i was restricted to $-0.5 < \eta_i < 2.5$. All jets are thus well contained in the LAr calorimeter. The measured kinematic region was restricted to $0.1 < y < 0.9$ and $Q^2 < 1\,\mathrm{GeV}^2$, as given by the acceptance for electrons in the LAr and Spacal. The kinematic range of the measured dijet cross sections is summarized in Table 1. Applying these cuts the total number of events measured was 5265.

$Q^2 < 1$ GeV^2
$0.1 < y < 0.9$
$E_{T,max} > 25$ GeV
$E_{T,second} > 15$ GeV
$-0.5 < \eta_i < 2.5$

Table 1: The definition of the phase space of the measured dijet cross sections.

3.3 Correction of the Data for Detector Effects

The data were corrected for detector effects such as limited resolution and inefficiencies. To determine these effects the HERWIG and PYTHIA Monte Carlo samples were used. Both programs do not describe the absolute normalization of the dijet cross sections. After scaling the HERWIG cross sections by 2 and the PYTHIA cross sections by 1.2 the two programs gave a good description of the measured jet distributions in shape and normalization.

The bin sizes of all distributions are matched to the resolution and result in good bin efficiency and purity. The correction was done by using the so called bin-to-bin method. The correction functions were calculated from the ratio of the cross sections with jets reconstructed from hadrons (hadron level) and from detector objects (detector level) in each bin, where each sample was subject to the selection criteria defined above. The correction functions of the two models are in good agreement and differ on average by 5% and at most by 20%. The mean values of the two Monte Carlo generators were thus taken for the correction. The resulting correction factors typically have values between 0.8 and 1.2.

3.4 Systematic Uncertainties

For the jet cross sections the following sources of systematic error were considered:

- A 2% uncertainty in the LAr energy scale results in an uncertainty of typically 10%.
- An 8% uncertainty in the hadronic Spacal energy scale results in an uncertainty of 1%.
- In addition to the variations of the calorimeter energy scales a shift of 1% on y is considered. This variation results in an uncertainty of 3%.
- Half of the difference between the correction factors calculated with HERWIG and with PYTHIA is taken as the uncertainty in the detector correction. The resulting uncertainty is less than 10%.
- The uncertainty in the trigger efficiency results in an error of ~ 3%.
- The uncertainty in the background subtraction results in an error of ~ 2%.
- The uncertainty in the integrated luminosity results in an overall normalization error of 1.5%.

The statistical and all systematic errors are added in quadrature. The resulting total uncertainty ranges from 10 to 30%, where the systematic contribution is dominated by uncertainties in the calorimeter energy scales and in the correction to the hadron level.

4 Results

The measured cross sections for inclusive dijet production in the reaction $ep \to e\,\mathrm{jet}\,\mathrm{jet}\,X$ are given as single differential cross sections in all cases. The data are corrected for detector effects and are presented at the level of stable hadrons for the phase space region defined in Table 1. The inner error bars of the data points in the figures denote the statistical, the outer error bars the total uncertainty. The data are also presented in Tables 2-7. All results are compared to next-to-leading order (NLO) QCD predictions obtained with the standard setting described in section 2 if not otherwise quoted. The predictions of NLO QCD corrected for hadronization effects NLO$(1 + \delta_{hadr})$ are also shown.

In Figure 1 the dijet cross section is shown as a function of the invariant mass M_{JJ} of the dijet system. The data are presented for M_{JJ} values between 45 and 180 GeV. The measured cross section falls by about 3 orders of magnitude over this range. NLO QCD describes the measured cross sections for the whole mass range. Hadronization corrections are less than 5% for all bins. The calculation using LO matrix elements fails to describe the low M_{JJ} region. This is partly due to the fact that the low M_{JJ} region is populated by events which are influenced by the asymmetric cuts on the jet transverse energies. Events in which the second jet has a transverse energy below 25 GeV contribute mainly in this region. In dijet calculations they only appear beyond leading order. The scale uncertainties in the QCD predictions are largest at low M_{JJ} values.

A similar statement on the large scale uncertainties and the difference between data and the LO calculation holds for small transverse momenta. In Figure 2a) the dijet cross section $d\sigma/dE_{T,mean}$ is shown. Here the scale uncertainties decrease from ± 20% for the first bins to less than ± 5% for $E_{T,mean} > 30$ GeV. The data are well described by the NLO calculation. The dijet cross section as a function of the transverse energy of the highest transverse energy jet $E_{T,max}$ is shown in Figure 2b). The distribution again demonstrates that the data are described by NLO QCD up to the highest $E_{T,max}$ values within errors. The NLO scale uncertainty is not reduced significantly with increasing $E_{T,max}$. The cross sections differential in transverse energy are hardly altered by hadronization corrections which are around 5% for all bins. The NLO QCD calculation with hadronization corrections predicts the measured cross sections up to the highest masses and transverse energies, although the photon and proton pdfs have been extracted from quite different processes and mostly at lower scales.

To further explore the photon and proton structure the differential cross section $d\sigma/d\overline{\eta}$ is displayed in Figure 3 for two ranges of $E_{T,max}$ subdivided into two y regions. While the former implies a variation of the scale the latter corresponds to different center of mass energies in the photon-proton-system. Again, good agreement between data and NLO QCD is observed taking into account the uncertainties in the calculations and in the data points. The predictions tend to lie above the data at low $\overline{\eta}$, where direct interactions dominate and hadronization corrections

are largest. At high $\overline{\eta}$, where in contrast resolved interactions dominate and hadronization corrections are small, the NLO QCD predictions agree well with the measured data.

Figures 4a) and b) show the dijet cross section $d\sigma/dx_\gamma$ as a function of x_γ for two different x_p regions. The calculations exceed the data, while remaining within the given uncertainties, only for $x_\gamma > 0.85$, where the largest hadronization correction occur. Using the MRST99 1-3 proton pdfs (with a large variation of the high x_p gluon density) instead of CTEQ5M results in differences of less than 5% for the predicted cross section for $x_p < 0.1$ and up to 15% for $x_p > 0.1$. This is smaller than the scale uncertainties for $x_p < 0.1$ and of the same order for $x_p > 0.1$. These findings are corroborated in Figures 4c) and d) where the cross section $d\sigma/dx_p$ is shown as a function of x_p for two different x_γ regions. Even at the highest x_p the measured cross sections are seen to agree well with the QCD predictions, which in this part of the phase space attribute about 40% of the cross section to processes induced by gluons in the proton. The constraints on the pdfs used in the QCD calculations here come dominantly from deeply inelastic scattering at lower scales where the gluon fraction is smaller. The concept of universal pdfs in hard processes in QCD is thus observed to describe measurements with rather different experimental conditions.

Figure 5 displays the dijet cross sections $d\sigma/dx_\gamma$ as a function of x_γ for two regions of $E_{T,max}$, representing different factorization scales for the photon and proton pdfs. The data are compared to NLO calculations corrected for hadronization effects with two different parameterizations of the photon structure. The predictions describe the data well and vary only slightly with the photon pdfs used. In contrast the NLO scale uncertainties produce a significant effect as can be inferred from Figure 6, which repeats the data of Figure 5 with a comparison of the GRV-HO pdfs of the photon. For high values of x_γ the hadronization corrections are sizeable and improve the agreement with the data. A more detailed comparison between data and theory is obtained by plotting their relative difference as shown in Figure 7. NLO predictions including hadronization corrections are shown for both sets of photon pdfs. At variance to the previous plots the error bars of the data contain only the uncorrelated systematic errors, while the correlated errors due to the uncertainty in the calorimeter energy scales are shown as a hatched band. Figure 7 shows that the assumed NLO scale uncertainties are the dominant source of uncertainties in the comparison of data and theory. The expectation exceeds the data only for the high x_γ and high $E_{T,max}$ regions. Within these uncertainties the picture of an universal photon structure is thus corroborated.

Finally, the dijet cross section $d\sigma/d\cos\theta^*$ is plotted in Figures 8a) and b) for $x_\gamma < 0.8$ and $x_\gamma > 0.8$ respectively. The cross section decreases with increasing $\cos\theta^*$ mainly because of the cuts in E_T. Again, the data are well described by NLO QCD for low x_γ, whereas at higher x_γ the predictions overshoot the data for small values of $\cos\theta^*$. These cross sections are also shown with a cut on the invariant mass M_{JJ} of the dijet system in Figures 8c) and d), essentially excluding the first bin of Figure 1. The cut reduces the restriction of the phase space due to the correlation with the E_T requirements and changes the shape of the distribution towards that expected from the QCD matrix elements. The QCD calculations reproduce this transition nicely in both x_γ regions where resolved and direct photon induced processes contribute with different weights.

5 Conclusions

New measurements of dijet cross sections in photoproduction at high transverse energies are presented for various jet kinematic observables. The measurements cover invariant dijet masses up to $180\,\text{GeV}$ and transverse energies up to $80\,\text{GeV}$, reaching x_p and x_γ values where the experimental information was previously limited. In this kinematic domain non-perturbative effects like multiple interactions and hadronization are found to be small, which allows a direct comparison of NLO QCD calculations with the data to be made. The results demonstrate the power of perturbative QCD in predicting the measured cross sections in a wide kinematical range. Even though the photon pdfs have been obtained from measurements at lower scales, their QCD evolution correctly reproduces the data at high scales. The data do not require significant changes in the parameterizations of the pdfs but are certainly useful to further constrain the existing ones. Likewise our understanding of the proton structure in the high x_p, high scale region can be improved with the help of these data. A future stronger constraint requires a reduction of both the theoretical scale uncertainties and the systematic uncertainties in the data.

Acknowledgements

We are grateful to the HERA machine group whose outstanding efforts have made and continue to make this experiment possible. We thank the engineers and technicians for their work in constructing and now maintaining the H1 detector, our funding agencies for financial support, the DESY technical staff for continual assistance, and the DESY directorate for the hospitality which they extend to the non-DESY members of the collaboration. We wish to thank S. Frixione and B. Pötter for many helpful discussions.

References

[1] T. Ahmed *et al.* [H1 Collaboration], Phys. Lett. B **297** (1992) 205.

[2] C. Adloff *et al.* [H1 Collaboration], Eur. Phys. J. C **1** (1998) 97 [arXiv:hep-ex/9709004].

[3] C. Adloff *et al.* [H1 Collaboration], Phys. Lett. B **483** (2000) 36 [arXiv:hep-ex/0003011].

[4] J. Breitweg *et al.* [ZEUS Collaboration], Eur. Phys. J. C **1** (1998) 109 [arXiv:hep-ex/9710018].

[5] J. Breitweg *et al.* [ZEUS Collaboration], Eur. Phys. J. C **11** (1999) 35 [arXiv:hep-ex/9905046].

[6] T. Affolder *et al.* [CDF Collaboration], Phys. Rev. D **64** (2001) 012001 [arXiv:hep-ex/0012013].

[7] V. M. Abazov *et al.* [D0 Collaboration], arXiv:hep-ex/0109041.

[8] R. Nisius, Phys. Rept. **332** (2000) 165 [arXiv:hep-ex/9912049].

[9] J. Huston, S. Kuhlmann, H. L. Lai, F. I. Olness, J. F. Owens, D. E. Soper and W. K. Tung, Phys. Rev. D **58** (1998) 114034 [arXiv:hep-ph/9801444].

[10] S. Chekanov *et al.* [ZEUS Collaboration], DESY 01-220, arXiv:hep-ex/0112029.

[11] P. Kessler, Il Nuovo Cimento **17** (1960) 809.

[12] V. M. Budnev, I. F. Ginzburg, G. V. Meledin and V. G. Serbo, Phys. Rept. **15** (1974) 181.

[13] S. Frixione, M. L. Mangano, P. Nason and G. Ridolfi, Phys. Lett. B **319** (1993) 339 [arXiv:hep-ph/9310350].

[14] S. Frixione and G. Ridolfi, Nucl. Phys. B **507** (1997) 315 [arXiv:hep-ph/9707345].

[15] M. Klasen and G. Kramer, Z. Phys. C **76** (1997) 67 [arXiv:hep-ph/9611450].

[16] B. W. Harris and J. F. Owens, Phys. Rev. D **56** (1997) 4007 [arXiv:hep-ph/9704324].

[17] P. Aurenche, L. Bourhis, M. Fontannaz and J. P. Guillet, Eur. Phys. J. C **17** (2000) 413 [arXiv:hep-ph/0006011].

[18] U. Baur, J. A. Vermaseren and D. Zeppenfeld, Nucl. Phys. B **375** (1992) 3.

[19] S. D. Ellis and D. E. Soper, Phys. Rev. D **48** (1993) 3160 [arXiv:hep-ph/9305266].

[20] S. Catani, Y. L. Dokshitzer, M. H. Seymour and B. R. Webber, Nucl. Phys. B **406** (1993) 187.

[21] C. Adloff *et al.* [H1 Collaboration], Eur. Phys. J. C **19** (2001) 289 [arXiv:hep-ex/0010054].

[22] T. Sjöstrand, Comput. Phys. Commun. **82** (1994) 74.

[23] G. Marchesini, B. R. Webber, G. Abbiendi, I. G. Knowles, M. H. Seymour and L. Stanco, Comput. Phys. Commun. **67** (1992) 465.

[24] R. Brun, F. Bruyant, M. Maire, A. C. McPherson and P. Zanarini, CERN-DD/EE/84-1.

[25] M. Glück, E. Reya and A. Vogt, Z. Phys. C **67** (1995) 433.

[26] M. Glück, E. Reya and A. Vogt, Phys. Rev. D **46** (1992) 1973.

[27] S. Frixione, Nucl. Phys. B **507** (1997) 295 [arXiv:hep-ph/9706545].

[28] H. L. Lai *et al.*, Phys. Rev. D **55** (1997) 1280 [arXiv:hep-ph/9606399].

[29] A. D. Martin, R. G. Roberts, W. J. Stirling and R. S. Thorne, Eur. Phys. J. C **14** (2000) 133 [arXiv:hep-ph/9907231].

[30] M. Glück, E. Reya and A. Vogt, Phys. Rev. D **45** (1992) 3986.

[31] P. Aurenche, J. P. Guillet and M. Fontannaz, Z. Phys. C **64** (1994) 621 [arXiv:hep-ph/9406382].

[32] I. Abt *et al.* [H1 Collaboration], Nucl. Instrum. Meth. A **386** (1997) 310.

[33] I. Abt *et al.* [H1 Collaboration], Nucl. Instrum. Meth. A **386** (1997) 348.

[34] B. Andrieu *et al.* [H1 Calorimeter Group Collaboration], Nucl. Instrum. Meth. A **336** (1993) 460.

[35] R. D. Appuhn *et al.* [H1 SPACAL Group Collaboration], Nucl. Instrum. Meth. A **386** (1997) 397.

[36] C. Adloff *et al.* [H1 Collaboration], Z. Phys. C **74** (1997) 221 [arXiv:hep-ex/9702003].

[37] A. Blondel and F. Jacquet, Proceedings of the Study of an ep Facility for Europe ed. U. Amaldi, DESY 79/48 (1979) 391.

[38] L. Lönnblad, Comput. Phys. Commun. **71** (1992) 15.

[39] K. Charchula, G. A. Schuler and H. Spiesberger, Comput. Phys. Commun. **81** (1994) 381.

M_{JJ} (GeV)	$\frac{d\sigma^{dijets}}{dM_{JJ}}$ (pb/GeV)	δ_{stat}(%)	$+\delta_{tot}$(%)	$-\delta_{tot}$(%)
45.-57.5	4.30	2.5	13	14
57.5-70.	3.69	2.9	11	11
70.-90.	1.33	3.7	13	11
90.-110.	0.39	6.9	12	16
110.-135.	0.101	12.	19	18
135.-180.	0.0102	27.1	32	30
$E_{T,mean}$ (GeV)	$\frac{d\sigma^{dijets}}{dE_{T,mean}}$ (pb/GeV)	δ_{stat}(%)	$+\delta_{tot}$(%)	$-\delta_{tot}$(%)
20.-30.	10.65	1.8	12	12
30.-45.	2.41	3.1	12	11
45.-60.	0.166	11.6	16	17
60.-80	0.0192	29.2	37	34
$E_{T,max}$ (GeV)	$\frac{d\sigma^{dijets}}{dE_{T,max}}$ (pb/GeV)	δ_{stat}(%)	$+\delta_{tot}$(%)	$-\delta_{tot}$(%)
25.-35.	12.36	1.8	11	12
35.-45.	1.82	3.9	12	12
45.-60.	0.252	8.4	15	15
60.-80.	0.0198	27.4	33	32

Table 2: Differential ep cross sections for dijet production as a function of the invariant dijet mass M_{JJ} (upper table), as a function of $E_{T,mean}$ (middle table) and as a function of $E_{T,max}$ (lower table) with statistical and total upper and lower uncertainties (cf. Figures 1 and 2).

$\overline{\eta}$	$\frac{d\sigma^{dijets}}{d\overline{\eta}}$ (pb)	δ_{stat}(%)	$+\delta_{tot}$(%)	$-\delta_{tot}$(%)
	$0.1 < y < 0.5$ and $25 < E_{T,max} < 35$ GeV			
0.6-0.9	7.55	10.0	20	22
0.9-1.3	42.2	4.4	11	15
1.3-1.7	52.2	4.2	10	11
1.7-2.1	31.8	5.4	12	11
2.1-2.5	10.3	10.1	17	18
	$0.1 < y < 0.5$ and $35 < E_{T,max} < 80$ GeV			
0.9-1.3	2.57	14.0	20	20
1.3-1.7	10.2	8.0	14	13
1.7-2.1	6.80	9.9	14	16
2.1-2.5	1.47	21.0	24	24
	$0.5 < y < 0.9$ and $25 < E_{T,max} < 35$ GeV			
0.0-0.6	27.9	4.7	17	14
0.6-0.9	66.4	4.5	13	13
0.9-1.3	43.9	4.9	14	11
1.3-1.7	20.8	7.4	13	16
1.7-2.1	10.2	11.7	14	14
2.1-2.5	2.75	24.8	30	29
	$0.5 < y < 0.9$ and $35 < E_{T,max} < 80$ GeV			
0.6-0.9	9.77	9.7	20	20
0.9-1.3	14.14	7.5	13	13
1.3-1.7	9.12	9.3	15	15
1.7-2.1	2.59	18.1	24	24

Table 3: Differential ep cross sections for dijet production as a function of $\overline{\eta}$ with statistical and total upper and lower uncertainties (cf. Figure 3).

x_γ	$\frac{d\sigma^{dijets}}{dx_\gamma}$ (pb)	δ_{stat}(%)	$+\delta_{tot}$(%)	$-\delta_{tot}$(%)
	$x_p < 0.1$			
0.5-0.7	33.5	7.5	20	20
0.7-0.85	75.0	5.8	19	14
0.85-1.	182.7	3.3	13	13
	$x_p > 0.1$			
0.1-0.3	41.4	8.0	15	16
0.3-0.5	78.9	5.1	13	13
0.5-0.7	87.2	4.5	12	12
0.7-0.85	126.8	4.3	12	12
0.85-1	256.1	3.0	10	12

Table 4: Differential ep cross sections for dijet production as a function of x_γ with statistical and total upper and lower uncertainties (cf. Figure 4).

x_p	$\frac{d\sigma^{dijets}}{dx_p}$ (pb)	δ_{stat}(%)	$+\delta_{tot}$(%)	$-\delta_{tot}$(%)
	$x_\gamma < 0.8$			
0.05-0.1	288.0	5.3	15	17
0.1-0.15	352.1	4.8	13	11
0.15-0.22	298.6	4.4	9	15
0.22-0.32	121.8	5.6	19	12
0.32-0.6	7.86	11.8	17	19
	$x_\gamma > 0.8$			
0.05-0.1	530.0	3.5	12	14
0.1-0.15	384.4	4.3	12	14
0.15-0.22	232.1	4.7	11	12
0.22-0.32	83.7	6.5	13	13
0.32-0.6	7.4	12.7	19	18

Table 5: Differential ep cross sections for dijet production as a function of x_p with statistical and total upper and lower uncertainties (cf. Figure 4).

x_γ	$\frac{d\sigma^{dijets}}{dx_\gamma}$ (pb)	δ_{stat}(%)	$+\delta_{tot}$(%)	$-\delta_{tot}$(%)
	$25 < E_{T,max} < 35$ GeV			
0.1-0.3	40.1	8.4	17	18
0.3-0.5	77.3	5.3	11	13
0.5-0.7	101.1	4.3	14	14
0.7-0.85	173.6	3.9	14	11
0.85-1.	361.7	2.5	11	12
	$35 < E_{T,max} < 80$ GeV			
0.1-0.3	2.34	27.5	34	31
0.3-0.5	9.83	12.1	17	18
0.5-0.7	19.7	8.5	14	15
0.7-0.85	28.7	8.0	15	16
0.85-1.	78.1	4.9	13	12

Table 6: Differential ep cross sections for dijet production as a function of x_γ with statistical and total upper and lower uncertainties (cf. Figures 5, 6 and 7).

$\cos\theta^*$	$\frac{d\sigma^{dijets}}{d\cos\theta^*}$ (pb)	δ_{stat}(%)	$+\delta_{tot}$(%)	$-\delta_{tot}$(%)
	$x_\gamma < 0.8$			
0.0-0.1	102.0	6.1	13	13
0.1-0.2	98.3	6.3	11	14
0.2-0.3	98.0	6.4	16	15
0.3-0.4	89.0	6.4	15	13
0.4-0.5	95.6	6.5	18	14
0.5-0.6	86.6	6.8	15	17
0.6-0.7	71.3	7.5	14	14
0.7-0.85	33.8	8.8	14	16
	$x_\gamma > 0.8$			
0.0-0.1	100.1	5.6	12	13
0.1-0.2	108.6	5.5	11	12
0.2-0.3	115.6	5.4	14	13
0.3-0.4	106.1	5.5	10	13
0.4-0.5	95.7	5.7	14	14
0.5-0.6	95.0	5.9	12	13
0.6-0.7	86.3	6.3	25	23
0.7-0.85	49.5	7.0	14	13
	$x_\gamma < 0.8$ and $M_{JJ} > 65$ GeV			
0.0-0.1	10.1	17.0	21	21
0.1-0.2	12.0	16.4	19	21
0.2-0.3	12.6	16.3	19	20
0.3-0.4	14.3	15.9	22	21
0.4-0.5	21.0	12.8	16	17
0.5-0.6	30.9	11.3	16	14
0.6-0.7	37.9	10.3	18	19
0.7-0.85	30.4	9.4	17	14
	$x_\gamma > 0.8$ and $M_{JJ} > 65$ GeV			
0.0-0.1	24.9	11.7	15	16
0.1-0.2	25.6	11.9	15	16
0.2-0.3	27.6	11.3	16	16
0.3-0.4	30.5	11.0	15	16
0.4-0.5	30.3	10.9	17	16
0.5-0.6	43.4	9.2	15	15
0.6-0.7	64.2	7.7	19	19
0.7-0.85	47.0	7.4	14	13

Table 7: Differential ep cross sections for dijet production as a function of $\cos\theta^*$ with statistical and total upper and lower uncertainties (cf. Figure 8).

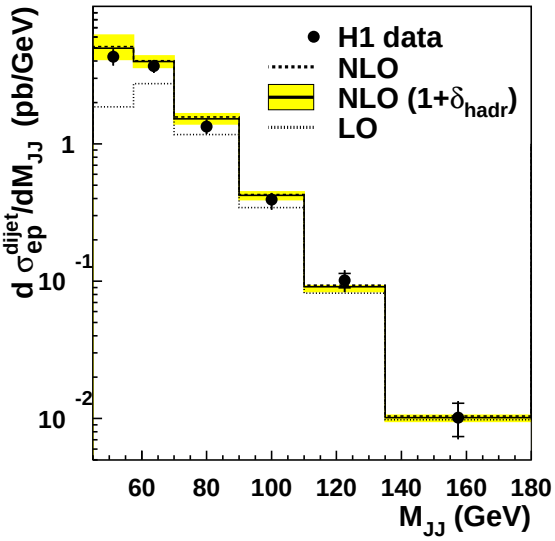

Figure 1: Differential ep cross sections for dijet production ($Q^2 < 1\text{GeV}^2$) as a function of the invariant dijet mass M_{JJ} of the two highest E_T jets. Here, as well as in the following figures unless explicitly stated otherwise, the inner error bars denote the statistical error, the outer error bars the total uncertainties of the data. The LO predictions using CTEQ5M pdfs for the proton and GRV-HO pdfs for the photon are shown as a dotted line. NLO predictions with the same pdfs are shown as a dashed line. The full line shows the NLO predictions, including hadronization corrections and the grey band indicates the renormalization and factorization scale uncertainties of the NLO prediction.

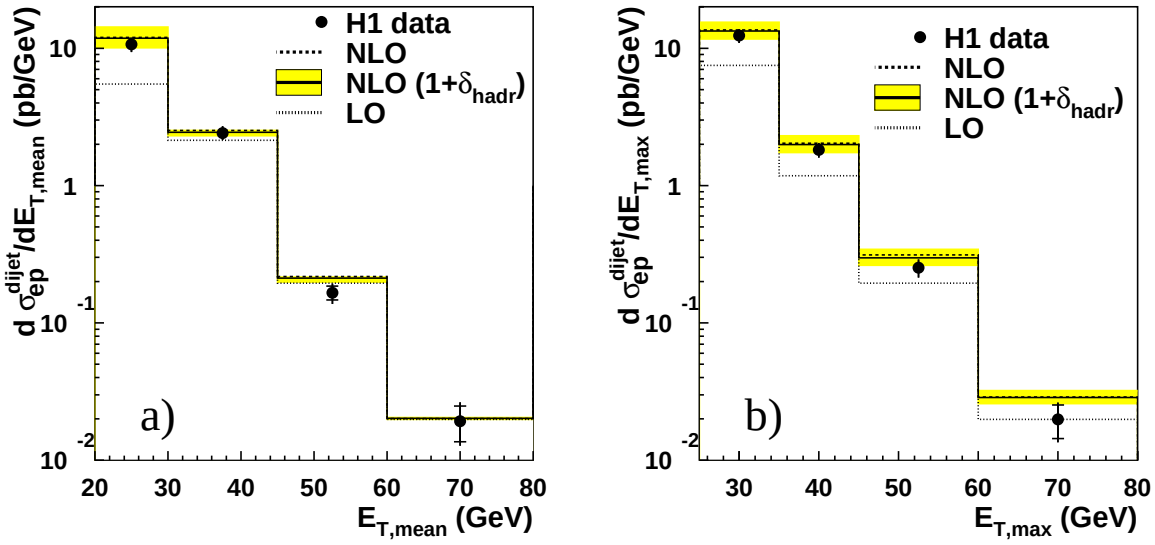

Figure 2: Differential ep cross sections for dijet production ($Q^2 < 1\text{GeV}^2$) as a function of a) $E_{T,mean}$, the mean and b) $E_{T,max}$, the maximum E_T of the two highest E_T jets. The LO predictions using CTEQ5M pdfs for the proton and GRV-HO pdfs for the photon are shown as a dotted line. NLO predictions with the same pdfs are shown as a dashed line. The full line shows the NLO predictions, including hadronization corrections and the grey band indicates the renormalization and factorization scale uncertainties of the NLO prediction.

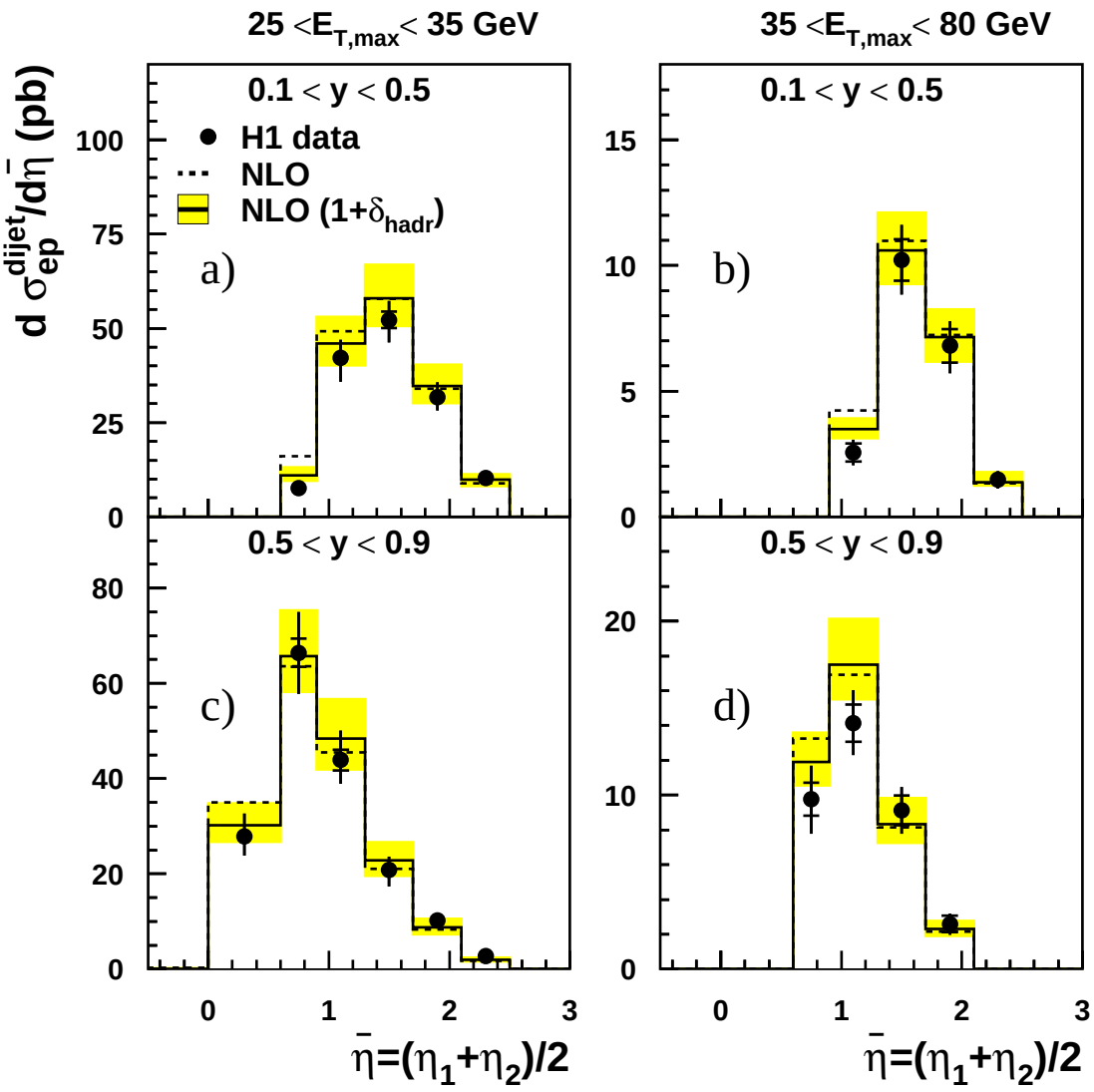

Figure 3: Differential ep cross sections for dijet production ($Q^2 < 1\text{GeV}^2$) as a function of the $\overline{\eta}$ of the two highest E_T jets. The regions of low y, a) and b) and high y, c) and d) are shown for two ranges of $E_{T,max}$. NLO predictions using CTEQ5M pdfs for the proton and GRV-HO pdfs for the photon are shown as a dashed line. The full line shows the NLO predictions, including hadronization corrections and the grey band indicates the renormalization and factorization scale uncertainties of the NLO prediction.

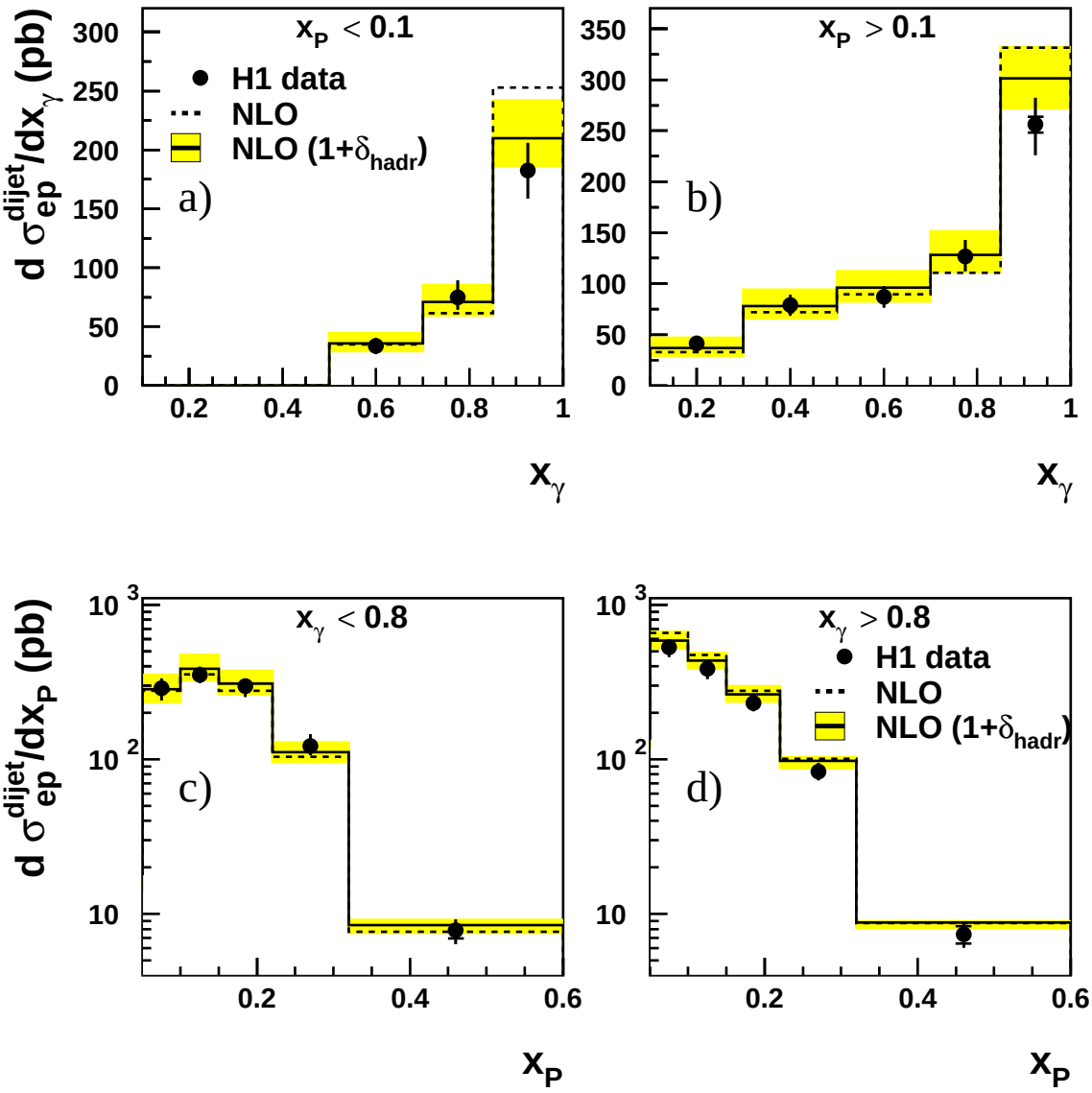

Figure 4: Differential ep cross sections for dijet production ($Q^2 < 1\text{GeV}^2$) as a function of x_γ a) and b) and x_p c) and d). Figures a) and b) distinguish regions of small and large x_p and figures c) and d) corresponding regions in x_γ. NLO predictions using CTEQ5M pdfs for the proton and GRV-HO pdfs for the photon are shown as a dashed line. The full line shows the NLO predictions, including hadronization corrections and the grey band indicates the renormalization and factorization scale uncertainties of the NLO prediction.

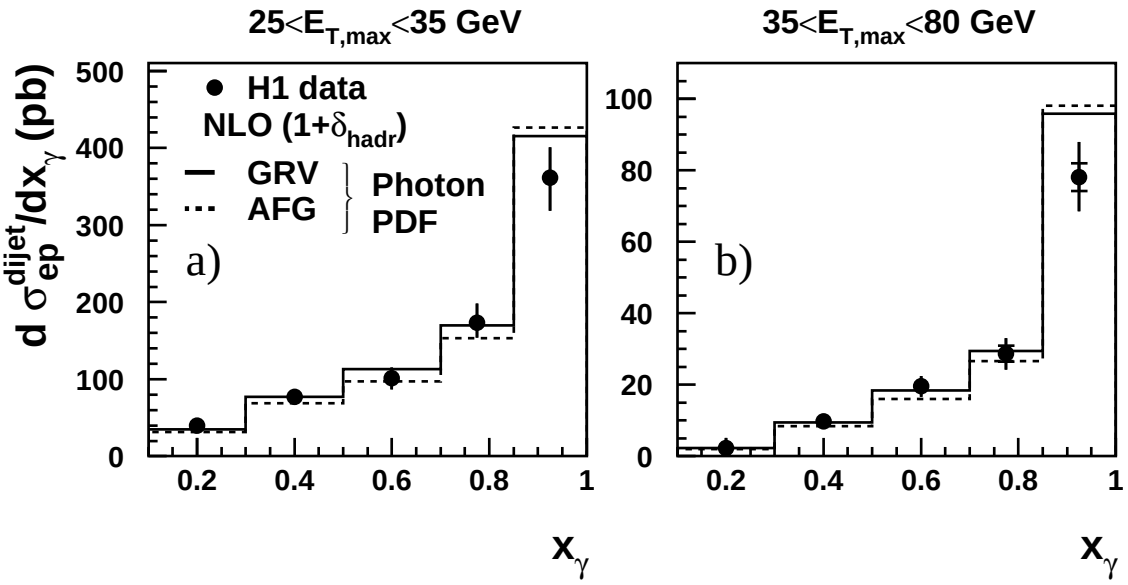

Figure 5: Differential ep cross sections for dijet production ($Q^2 < 1\text{GeV}^2$) as a function of x_γ for a) low $E_{T,max}$ and b) high $E_{T,max}$. The NLO predictions using CTEQ5M pdfs for the proton and GRV-HO pdfs for the photon and including hadronization corrections are shown as a full line. NLO predictions using AFG-HO parametrizations of the photon pdfs and including hadronization corrections are shown as the dashed line.

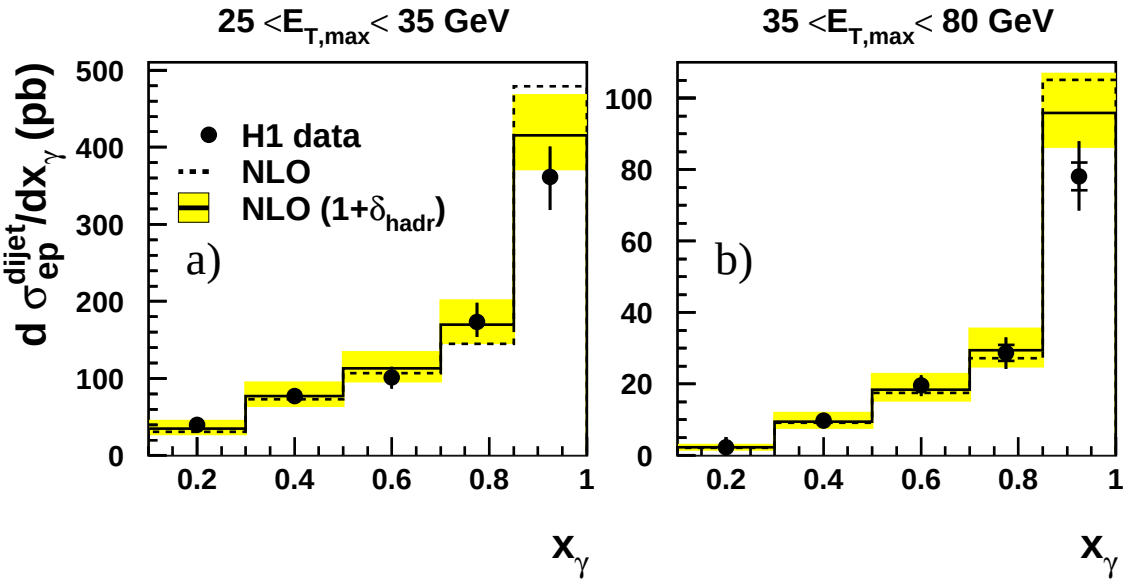

Figure 6: Differential ep cross sections for dijet production ($Q^2 < 1\text{GeV}^2$) as a function of x_γ for a) low $E_{T,max}$ and b) high $E_{T,max}$. NLO predictions using CTEQ5M pdfs for the proton and GRV-HO pdfs for the photon are shown as a dashed line. The full line shows the NLO predictions, including hadronization corrections and the grey band indicates the renormalization and factorization scale uncertainties of the NLO prediction.

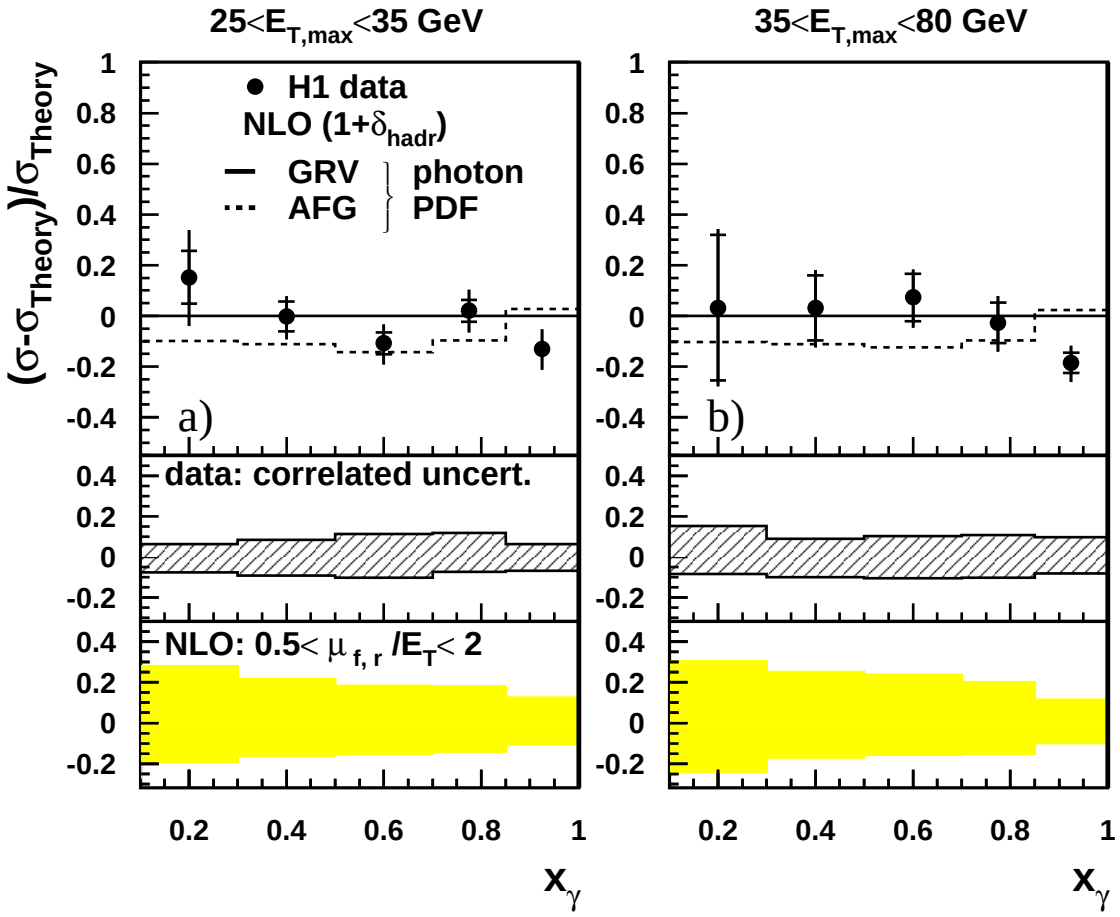

Figure 7: The x_γ dependence of the relative difference of the measured dijet cross sections ($Q^2 < 1\text{GeV}^2$) from the NLO prediction, with hadronization corrections applied using CTEQ5M pdfs for the proton and GRV-HO pdfs for the photon (here σ_{Theory}). The symbol σ stands for $d\sigma/dx_\gamma$. Shown is the relative difference of the data (points) and the NLO predictions using the AFG-HO pdf (dashed line) with hadronization corrections applied. Figures a) and b) show the relative difference for the lower $E_{T,max}$ and higher $E_{T,max}$ regions respectively. The inner error bars denote the statistical error, the outer error bars denote all statistical and uncorrelated systematic errors of the data added in quadrature. The correlated systematic errors are shown in the middle plots as a shaded band. The grey band (lower plots) shows the renormalization and factorization scale uncertainties of this NLO prediction.

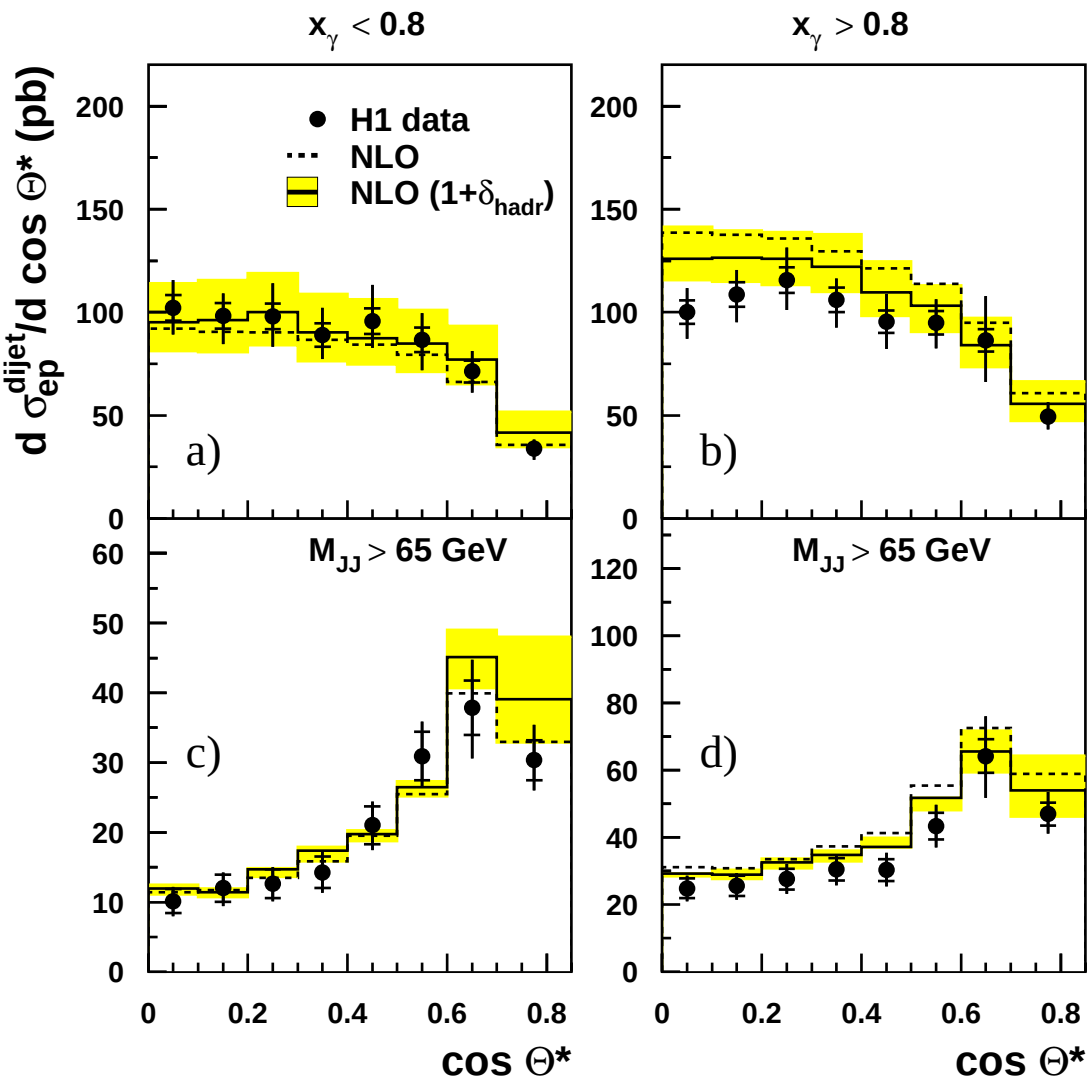

Figure 8: Differential ep cross sections for dijet production ($Q^2 < 1\text{GeV}^2$) as a function of $\cos\theta^*$ distinguished for small x_γ a) and c) and large x_γ b) and d). Figures c) and d) show the cross sections for large invariant masses of the dijet system. NLO predictions using CTEQ5M pdfs for the proton and GRV-HO pdfs for the photon are shown as a dashed line. The full line shows the NLO predictions, including hadronization corrections and the grey band indicates the renormalization and factorization scale uncertainties of the NLO prediction.